Journal of Molecular Structure 1014 (2012) 17–25

Contents lists available at SciVerse ScienceDirect

Journal of Molecular Structure

journal homepage: www.elsevier.com/locate/molstruc

Synthesis and spectroscopic characterization of gallic acid and some of its azo complexes

Mamdouh S. Masoud [a], Sawsan S. Hagagg [a], Alaa E. Ali [b,*], Nessma M. Nasr [c]

[a] Chemistry Department, Faculty of Science, Alexandria University, Alexandria, Egypt
[b] Chemistry Department, Faculty of Science, Damanhour University, Damanhour, Egypt
[c] Science Park for Pharmaceuticals, Faculty of Pharmacy, Alexandria University, Alexandria, Egypt

ARTICLE INFO

Article history:
Received 5 October 2011
Received in revised form 25 January 2012
Accepted 25 January 2012
Available online 4 February 2012

Keywords:
Gallic acid complexes
Azo derivatives
IR
UV spectroscopy
Biological activity
Thermal analysis

ABSTRACT

A series of gallic acid and azo gallic acid complexes were prepared and characterized by elemental analysis, IR, electronic spectra and magnetic susceptibility. The complexes were of different geometries: Octahedral, Tetrahedral and Square Planar. ESR was studied for copper complexes. All of the prepared complexes were of isotropic nature. The thermal analyses of the complexes were studied by DTA and DSC techniques. The thermodynamic parameters and the thermal transitions, such as glass transitions, crystallization and melting temperatures for some ligands and their complexes were evaluated and discussed. The entropy change values, $\Delta S^{\#}$, showed that the transition states are more ordered than the reacting complexes. The biological activities of some ligands and their complexes are tested against Gram positive and Gram negative bacteria. The results showed that some complexes have a well considerable activity against different organisms.

1. Introduction

Gallic acid, an organic acid, known as 3,4,5-trihydroxybenzoic acid ($C_6H_2(OH)_3COOH$), is found widely throughout the plant kingdom. High gallic acid contents can be found in gallnuts, grapes, sumac, witch hazel, tea leaves, hops, and oak bark. Gallic acid exists in two forms as the free molecule and as part of tannins. Pure gallic acid is a colorless crystalline organic powder, salts and esters of gallic acid are termed gallates [1]. It has many applications in chemical research and industry such as being used as a standard for determining the phenol content of various analytes by the Folin–Ciocalteau assay [2] and also used for making dyes and inks [3].

Gallic acid is commonly used in the pharmaceutical industry because many in vivo and in vitro studies in humans, animals, and cell culture have provided evidence for the following actions of gallic acid. It shows cytotoxicity against cancer cells, without harming healthy cells [4] and it can be used to treat albuminuria and diabetes [5], also it seems to have antifungal and antiviral properties [6], which is used as an antioxidant and helps to protect human cells against oxidative damage [7]. It can be used as a remote astringent in cases of internal hemorrhage [8] and can also used to treat psoriasis and external hemorrhoids containing gallic acid [9]. Gallic acid molecule is essentially planar and has two intramolecular hydrogen bonds between hydroxyl groups, the hydrogen atoms of the three hydroxyl groups are oriented in the same direction around the ring and form intra-and intermolecular hydrogen bonds. The crystal structure is stabilized by all available intermolecular hydrogen bonds [10]. The two adjacent hydroxyl groups are engaged in a complex [11] and the remaining hydroxyl group is suggested to form hydrogen bonding with COO^- of the other legend presented on the same molecule forming a ring like structure.

Gallic acid is a strong chelating agent and forms complexes of high stability with iron [12,13]. The complex starts from pH = 3 and continues to pH = 9. The degree of chelating increases as the pH increase. Iron is attached to gallic acid through two adjacent hydroxyl groups presented on aromatic ring. Neodymium gallates were reported as a solid in which, metal to legend ratio was 1:2 and phenolic hydroxyl group vibrations were defined at 1282 and 1212 cm^{-1} [14]. Complexes of lanthanides (III), from (La—Lu) and Y (III) with gallic acid were obtained as solids with general formula Ln $(C_7H_5O_5)$ $(C_7H_4O_5)\cdot nH_2O$ (n = 2 for La—Ho and Y:n = 0 for (Er—Lu). The infrared spectrum of gallic acid shows a sharp absorption band of carboxylic group —COOH at 1664 cm^{-1} [14], absorption bands of δ_{OH} at 1428 and at 864 cm^{-1} as well as ν_{C-OH} at 1320 cm^{-1}, while, lanthanides gallic acid complexes give $\nu_{as\ OCO^-}$ at 1544–1528 cm^{-1} and $\nu_{as\ OCO^-}$ for dihydrated complexes, which are shifted to lower frequencies of about 8–12 cm^{-1} and have not changed their position for anhydrous complexes (Er—Lu).

* Corresponding author. Tel.: +20 111 5799866.
E-mail address: dralaae@yahoo.com (A.E. Ali).

0022-2860/$ - see front matter © 2012 Elsevier B.V. All rights reserved.
doi:10.1016/j.molstruc.2012.01.041

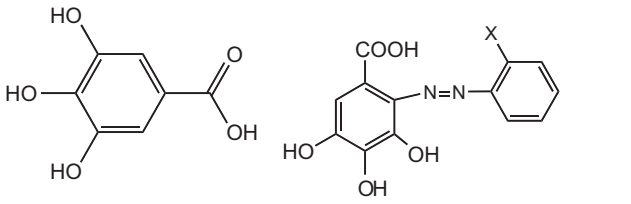

Fig. 1. The structure of gallic acid and its azo derivatives.

2. Experimental

2.1. Synthesis of azo legends and their metal complexes

All the organic compounds (I) were prepared in a similar way using the usual diazotization process [15]. The following abbreviations are given for the compounds under investigation: gallic acid [H_4L^1], 2-(phenyl azo 3,4,5-trihydroxy benzoic acid) [H_4L^2], 2-(2-hydroxy phenyl azo 3,4,5-trihydroxy benzoic acid) [H_5L^3] and 2-(2-carboxy phenyl azo 3,4,5-trihydroxy benzoic acid) [H_5L^4]. The structures of gallic acid and its azo derivatives are represented in Fig. 1. Manganese, cobalt, nickel, copper, zinc, cadmium and uranyl complexes were prepared by mixing 0.01 mol of metal chloride salt in an ammonia solution. The reaction mixture was refluxed for 1 h. The resulting solid complexes were removed by filtration, then washed several times with water–ethanol and dried under vacuum over $CaCl_2$ .The metal content was determined by atomic absorption technique, titrimetric with standard EDTA solution using the appropriate indicator [15]. The elemental analysis data for the complexes are given in Tables 1 and 2.

2.2. Physical measurements

The KBr disk infrared spectra were recorded on Perkin–Elmer 1430 spectrophotometer. The electronic spectra were measured by using Perkin Elmer spectrophotometer, model Lambda 4B, covering the range 200–900 nm. Molar magnetic susceptibilities, corrected for diamagnetism using Pascal's constants, were determined at room temperature (298 °K) using faraday's method .The apparatus was calibrated with Hg [Co (SCN)$_4$]. The ESR spectra of the copper complexes were recorded with a reflection spectrometer operating at 9.75 GHz (X-Band) in a cylindrical resonance cavity with 100 kHz modulation. The g-values were determined by comparison with DPPH signal (g = 2.0037). Thermal analysis (DAT and DSC) were carried out in the temperature range 25–500 °C, and the rate of heating was 10 °C/min.

The order of chemical reactions (n) was calculated via the peak symmetry method by Kissinger [16,38]. The value of the decomposed substance fraction, (α_m), at the moment of maximum development of reaction with $T = T_m$ was determined from the relation [17,39,18,40].

$$(1-\alpha_m) = n^{\frac{1}{1-n}}$$

The values of collision factor, Z, are obtained from the following equation:

$$z = \frac{E}{RT_m}\phi \exp\left(\frac{E}{RT_m^2}\right) = \frac{kT_m}{h}\exp\left(\frac{\Delta S^{\#}}{R}\right)$$

where, $\Delta S^{\#}$ represents the entropy of activation, R represents molar gas constant, ϕ represents rate of heating (K s^{-1}), k represents the Boltzmann constant and h represents the Planck's constant [19,41]. The heat of transformation $\Delta H^{\#}$, can be calculated from the DTA curves [20,42]. In general, the change in enthalpy ($\Delta H^{\#}$) for any phase of transformation taking place at any peak temperature T_m can be given by the following equation: $\Delta S^{\#} = \Delta H^{\#}/T_m$.

Table 1
Elemental analysis data, EAS and room temperature (298°K) magnetic moment values for H_4L^1 complexes.

Complex	% Calculated/(found)			λ (nm)	μ_{eff}	Geometry
	M	C	H			
Mn (H_2L^1)·4H_2O	18.6 (18.2)	28.4 (28.9)	4.0 (4.4)	300, 390, 450, 510	5.4	Octahedral
Co (H_2L^1)·2H_2O	22.4 (22.0)	31.9 (32.1)	3.0 (3.4)	300, 389, 675	4.6	Tetrahedral
Ni (H_3L^1)$_2$·4H_2O	12.4 (11.9)	35.8 (36.4)	3.8 (4.2)	286, 314, 350, 460, 510	3.8	Octahedral
Cu (H_2L^1)·4H_2O	22.0 (21.7)	29.2 (29.8)	4.1 (4.5)	400, 485, 510, 565	1.73	Square planar
Zn (H_2L^1)·3H_2O	22.7 (22.3)	29.2 (29.7)	4.1 (4.6)	300, 382, 486, 564	0.00	Tetrahedral
Cd (H_2L^1)·4H_2O	31.9 (32.6)	23.8 (24.2)	3.4 (3.7)	260, 450, 470	0.00	Tetrahedral
UO_2 (H_2L^1)·2H_2O	50.2 (49.8)	17.7 (18.1)	1.7 (1.6)	300, 400, 500	0.00	Octahedral

Table 2
Elemental analysis data, EAS and room temperature (298°K) magnetic moment values for the prepared azo gallic acid complexes.

Complex	% Calculated (found)					λ (nm)	μ_{eff}	Geometry
	M	C	H	N	X			
Co (H_3L^2) (H_4L^2) Cl·4H_2O	7.9 (8.0)	43.9 (44.1)	3.3 (3.3)	7.8 (7.4)	4.9 (5.1)	282, 375, 565	5.20	Octahedral
Ni (H_3L^2) (H_4L^2) Cl·4H_2O	8.2 (7.9)	43.9 (44.1)	3.3 (3.6)	7.8 (8.5)	4.9 5.1)	274, 370, 470, 580	3.36	Octahedral
Cu (H_4L^2)Cl_2·6H_2O	12.3 (12.0)	30.3 (30.7)	3.8 (4.4)	5.4 (6.1)	13.6 (14.1)	300, 370, 485, 545	1.81	Square planar
NiCu(H_2L^2)$_2$ (H_4L^2)·2H_2O	Cu 6.5 (6.8) Ni 6.0 (5.3)	47.9 (48.1)	3.0 (3.5)	8.6 (9.7)	–	300, 370, 470, 546	4.60	Octahedral
Co (H_5L^3)·Cl_2·6H_2O	11.2 (11.0)	29.7 (30.8)	3.8 (4.2)	5.3)5.6)	13.3 (13.6)	350, 540, 600, 630	5.20	Octahedral
Ni (H_5L^3)Cl_2·6H_2O	11.1 (11.2)	29.7 (30.2)	3.8 (4.1)	5.3 (5.7)	13.3 (13.7)	350, 535, 580, 606	3.60	Octahedral
Cu (H_5L^3)Cl_2·3H_2O	13.4 (13.3)	32.8 (33.2)	2.9 (3.5)	5.8 (6.1)	14.7 (14.3)	325, 400, 630	1.75	Square planar
Co (H_3L^4)·5H_2O	13.1 (12.8)	36.1 (36.6)	3.4 (3.6)	6.0 (6.4)	–	306, 390, 556	5.10	Tetrahedral
Ni (H_3L^4)·4H_2O	13.1 (13.2)	37.6 (38.1)	3.5 (3.7)	6.2 (6.6)	–	300, 400, 475	3.70	Octahedral
Cu (H_3L^4)·6H_2O	13.0 (12.7)	34.4 (34.8)	4.1 (4.4)	5.7 (5.9)	–	300, 400, 530	1.78	Square planar
Cd (H_3L^4)·2H_2O	24.2 (24.5)	36.1 (36.5)	2.5 (2.8)	6.0 (6.4)	–	300, 450	0.00	Tetrahedral

Table 3
Fundamental infrared bands (cm^{-1}) of H_4L^1 and its azo complexes.

Compound	ν_{OH}	$\nu_{C=O}$	$\nu_{C=C}$ and ν_{C-C}	ν_{C-OH} and δ_{OH}	δ_{C-OH}	$\delta_{C=O}$	γ_{O-H}	γ_{CO}	H. bonding OH in COOH
H_4L^1	3494 3279 2669	1666	1612 1540 1426	1318 1384	1266 1098	634	865 794	558	733
Mn $(H_2L^1)\cdot 4H_2O$	3429 3287 –	1639	1593 – –	– 1388	–	–	– 793	–	–
Co $(H_2L^1)\cdot H_2O$	3417 3295	–	1606 1574	– 1383	–	651	– 797	–	–
Ni $(H_3L^1)_2\cdot 4H_2O$	3446 3263	–	– 1588	– 1383	– 1115	668	–	–	–
Cu $(H_2L^1)\cdot 4H_2O$	3449 2664	–	1597 –	1393 –	–	680	–	–	760
Zn $(H_2L^1)\cdot 3H_2O$	3460 – 2664	–	– 1563 –	– 1384	– 1116	–	– 792	–	–
Cd $(H_2L^1)\cdot 4H_2O$	3665 3340 –	–	1595 1554 –	–	–	636	– 791	–	–
UO_2 $(H_2L^1)\cdot 2H_2O$	3398 – 2705	–	1615 1514 1431	1344 –	1260 1097	672	–	–	767

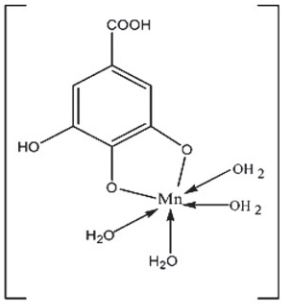

Mn (H_2L^1). $4H_2O$, Oh

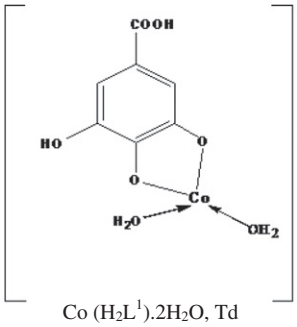

Co $(H_2L^1).2H_2O$, Td

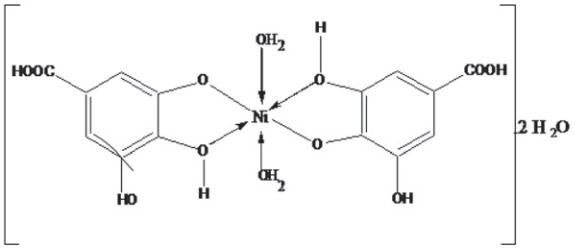

Ni $(H_3L^1)_2$ $.4H_2O$, Oh

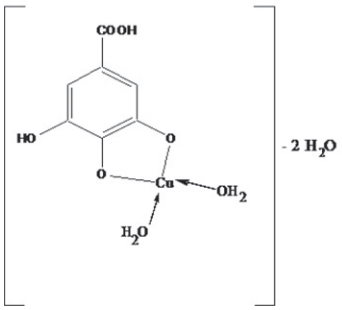

Cu (H_2L^1). $4H_2O$, SP

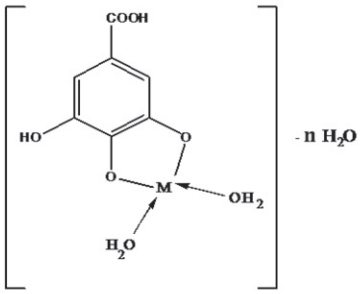

M = Cd, Zn
Zn (H_2L^1). $3H_2O$, Td n = 1
Cd $(H_2L^1).4H_2O$ Td, n = 2

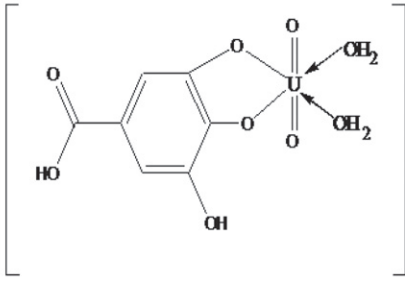

UO_2 $(H_2L^1).2$ H_2O, Oh

Fig. 2. The structures of the prepared gallic acid complexes.

3. Results and discussion

3.1. Infrared, electronic spectra and magnetic susceptibility of gallic acid and its complexes

Table 3 collects the infrared spectra of gallic acid and its complexes. Three bands were detected at 3494, 3279 and 2669 cm^{-1}, which are assigned to $\nu_{OH.}$ In case of manganese, cobalt, nickel, zinc and cadmium complexes, the first two peaks shifted from their positions and the third disappeared, whereas phenolic hydroxyl groups participated in forming the complexes [21]. The $\nu_{C=O}$ of the free legend is identified at 1666 cm^{-1}. This band is absent in case of cobalt, nickel, copper, zinc, cadmium and uranyl complexes. In case of manganese complex, the $\nu_{C=O}$ is shifted to lower frequency of about 27 cm^{-1}. Such data are in favor of suggesting that the carbonyl group is strongly affected on coordination with transition [22]. H_4L^1 gave δ_{OH}, γ_{OH} and ν_{C-O} modes of vibrations. Such data favored the carboxylate radical as possible oxidation of the phenolic hydroxyl with the formation of quinone structure [23]. These bands are affected on coordination with metal ions, to pinpoint that the oxygen atom is a center for coordination with the metal ions, also $\delta_{C=O}$ is a strong indicative that oxygen atom interact with metal ions. The different modes of vibrations of C—C, C=C and C—H are affected the complex, probably due to the aromaticity of the formed chelate is different from the legend [23]. he uranyl complex exhibits two bands at 942 and 825 cm^{-1}, which are assigned to the asymmetric stretching frequency ν_3 and symmetric stretching frequency (ν_1), respectively, of the dioxouranium ion [24]. The ν_3 value is used for the calculation of the force constant (F) [25] for the bonding sites of the O=U=O as follows: $(\nu_3)^2 = (1307)^2 \times (F_{U-O}/14.103$, $_{FU-O}$ value is found to be 7.3 m dyne A^{-1} and $R_{U-O} = 1.08\ (F_{U-O})^{-1/3} + 1.17$. Also, the U—O bond distance, R_{U-O} is calculated [26] and equals to 1.72 Å. The EAS of the black manganese-complex, [Mn $(H_2L^1)\cdot 4H_2O$], gave four bands. The first two peaks were at 300 and 350 nm, which are assigned to $^6A_{1g} \rightarrow {}^4A_{1g}$, while the third at 450 nm and that is due to

Table 4
Fundamental infrared bands (cm^{-1}) of H_4L^2, and its complexes.

Compound	ν_{OH}	$\nu_{C=O}$	$\nu_{C=C}$ and ν_{C-C}	$\nu_{N=N}$	$\delta_{C=O}$ and γ_{CO}	γ_{O-H}	H. bonding OH in COOH	ν_{M-O}	$_{M-N}$
H_4L^2	3452 3218 3033	1670	1595 1445	1493	690	835	750	–	–
Co (H_3L^2) (H_4L^2) $Cl\cdot 4H_2O$	3340 3060	–	1591 –	1506	692	833	744	513	609
Ni (H_3L^2) (H_4L^2) $Cl\cdot 4H_2O$	3352 3060	–	1587 –	1504	694	–	746	511	613
Cu $(H_4L^2)Cl_2\cdot 6H_2O$	3433 3344 3058	–	1589 –	1498	696	839	750	507	–
Ni Cu $(H_2L^2)_2$ $(H_4L^2)\cdot 2H_2O$	3367 3056	–	1589 –	1498	694	–	756	478	621

Table 5
Fundamental infrared bands (cm^{-1}) of H_5L^3 and its complexes.

Compound	ν_{OH}	$\nu_{C=O}$	$\nu_{C=C}$ and ν_{C-C}	$\nu_{N=N}$	$\delta_{C=O}$ and γ_{CO}	γ_{O-H}	H. bonding OH in COOH	ν_{M-O}	$_{M-N}$
H_5L^3	3312	1681	1606 1518	1452 –	663	818	753	–	–
Co $(H_5L^3)\cdot Cl_2\cdot 6H_2O$	3344	1654	1604 –	1451	668	–	756	592	640
$Ni(H_3L^4)\cdot 4H_2O$	3340	–	1597 1568	1383	1114	680	761	445	541
Cu $(H_3L^4)\cdot 6H_2O$	3342	1599 1446	–	1383	1117	696	764	446	534

Table 6
Fundamental infrared bands (cm^{-1}) of H_5L^4 and its complexes.

Compound	ν_{OH}	$\nu_{C=C}$ and ν_{C-C}	$\nu_{N=N}$	ν_{C-OH} and δ_{OH}	$\delta_{C=O}$ and γ_{CO}	γ_{O-H}	H. bonding OH in COOH	ν_{M-O}	ν_{M-N}
H_5L^4	3367 3203 3072	1710	1601 1452	1491	688	879	758	–	–
Co $(H_3L^4)\cdot 5H_2O$	3321 3224 3217	–	1575 –	–	687	–	759	445	503
Ni $(H_3L^4)\cdot 4H_2O$	3340	1597 1568	–	– 1383	680	–	761	445	541
Cu $(H_3L^4)\cdot 6H_2O$	3342 –	1599 1446	–	– 1383	696	839	764	446	534
Cd $(H_3L^4)\cdot 2H_2O$	3406 –	1579	–	– 1388	684	–	759	437	511

$^6A_{1g} \rightarrow {}^4T_{2g}$ transition, and the last band was at 510 nm, which is assigned to $^6A_{1g} \rightarrow {}^4T_{1g}$ transition [27,28]. Their room temperature μ_{eff} value of 5.4 B.M typified the existence of Octahedral configuration. The black cobalt-complex, [Co $(H_2L^1)\cdot 2H_2O$] gave three bands

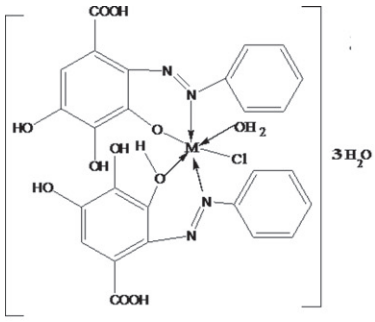

M = Ni, Co
Co (H_3L^2) (H_4L^2) Cl.$4H_2O$, Oh
Ni (H_3L^2) (H_4L^2) Cl.$4H_2O$, Oh

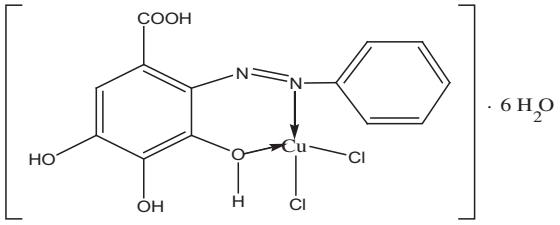

Cu $(H_4L^2)Cl_2$. $6H_2O$, SP

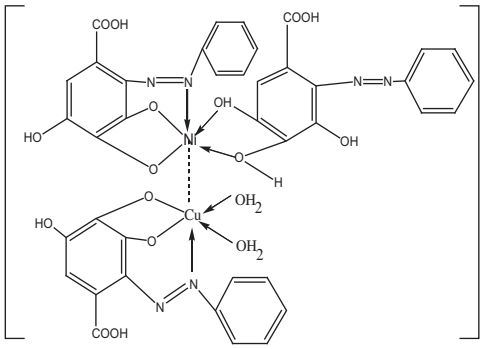

Ni $Cu(H_2L^2)_2$ $(H_4L^2)2H_2O$, Oh

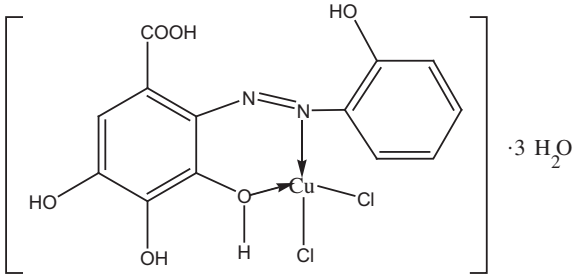

Cu $(H_5L^3)Cl_2$. $3H_2O$, Td

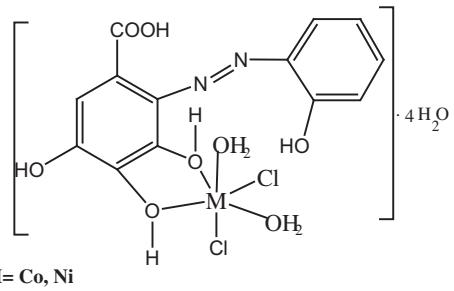

M= Co, Ni

Co (H_5L^3) .Cl_2.$6H_2O$, Oh
Ni $(H_5L^3)Cl_2$.$6H_2O$, Oh

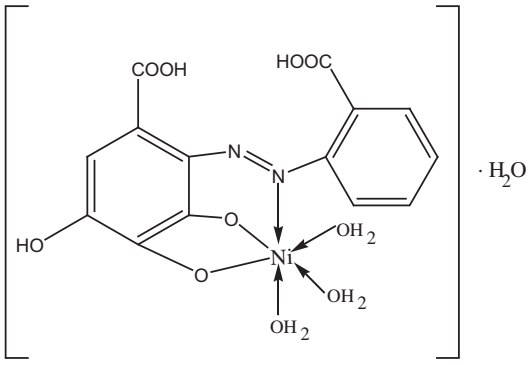

Ni (H_3L^4).$4H_2O$, Oh

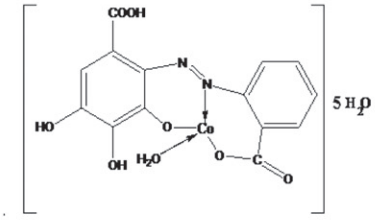

Co (H_3L^4). $5H_2O$

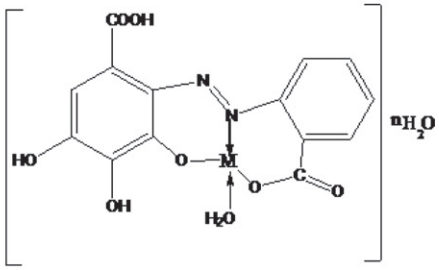

M= Cu , Cd

Cu (H3L4). 6H2O, SP n=5
Cd (H3L4). 2H2O, Td n= 1

Fig. 3. The structures of the prepared azo gallic acid complexes.

at 300, 389 and 675 nm (broad in nature), $^4A_2 \rightarrow {}^4T_1$ (P) transition of T_d structure [29]. Their room temperature μ_{eff} value of 4.6 B.M verified such geometry. The black nickel-complex, [Ni (H_2L^1) (H_4L^1) .$4H_2O$] gave five bands at 286, 314, 320, 460 and 510 nm and their μ_{eff} value, which equals 3.8 B.M of Octahedral structure [30]. The black copper-complex, [Cu $(H_2L^1)\cdot 4H_2O$] gave four bands at 400, 485, 510 and 565 nm, typified the presence of Square Planar stereochemistry mainly of $^2B_{1g} \rightarrow {}^2B_{2g}$ electronic transition in D_{4h} symmetry [31]. The room temperature magnetic moment value, μ_{eff}, is 1.73 B.M. The black zinc and cadmium complexes, [Zn $(H_2L^1)\cdot 3H_2O$], [Cd $(H_2L^1)\cdot 4H_2O$], respectively, gave four bands at 300, 382, 486 and 564 nm for zinc complex and three bands at 260, 450 and 470 nm for cadmium complex. Both complexes are diamagnetic. The EAS of the brown uranyl-complex, [UO_2 $(H_2L^1)\cdot 2H_2O$] gave three bands, the first two peaks were at 300 and 400 of charge transfer, probably ligand $\rightarrow O_{dbnd}U{=}O$, while the last band at 500 nm can be definitely assigned to the $^1\sum_g^+ \rightarrow {}^2\pi_4$ transition [32].

From the analytical data, and the foregoing spectral and magnetic moment results, gallic acid is of bidentate attachment through two oxygen atoms in the hydroxyl group on the reaction with transition metal salts of Mn (II), Co (II), Ni (II), Cu (II), Zn (II), Cd (II), UO_2 (II) and so the structures are suggested as in Fig. 2.

3.2. Infrared, electronic spectra and magnetic studies of azo gallic acid complexes

The fundamental bands of azo gallic acid compounds and their complexes are given in Tables 4–6. By comparing the infrared spectra of the complexes with that of the free legend, it should be possible to determine the binding sites. The vibration frequencies of coordinated functional groups (e.g. νOH, νC=O, δO—H, N=N,...) were affected with different degrees. In case of H_4L^2 and H_5L^4, three bands appeared at 3452, 3218, 3033 cm^{-1} and 3367, 3203, 3072 cm^{-1}, respectively. While H_5L^3 legend gave a broad band at 3312 cm^{-1}, which is assigned to ν_{OH}, [33–35] (Tables 4 and 5). Some changes occurred on the complex, the data in such region are related either to the —OH group which affected the coordination or to the existence of water molecule. Hydrogen bonded structures were expected due to intra-molecular H-bonding between the azo group and the o-carboxy H-bonding of the type O—H···N between the —OH or —COOH substituent and the N=N group [36–39]. The $\nu_{C=O}$ of H_4L^2, H_5L^3 and H_5L^4 legends are at 1670, 1681 and 1710 cm^{-1}, respectively [22]. This peak was absent in all complexes, suggesting that the carbonyl group is strongly affect the coordination with transition metal ions either by direct interaction between the lone pair of electrons of the carbonyl group with metal ion or through tautomerization. Also, $\delta_{C=O}$ vibration band led to the same conclusion. H_4L^2, H_5L^3 and H_5L^4 compounds gave bands at 1493, 1452 and 1491 cm^{-1}, respectively, which identified the azo vibration [36–38]. The shift of this band in all complexes indicated that the azo group is involved in coordination. The presence of $\gamma_{C=O}$, $\nu_{C=O}$ modes of vibrations in the metal complexes, suggests that the oxygen atom is also a center of coordination [23]. New bands appeared in all azo gallic acid complexes in the frequency ranges 437–592 cm^{-1} and 503–640 cm^{-1}, which are attributed to ν_{M-N} and ν_{M-O}, respectively. Table 1 illustrates the spectral, electronic transitions and magnetic properties of the complexes. The data indicated the existence of most complexes in Octahedral and Tetrahedral geometries [29,31,40], except the copper complexes which is Square Planar. From the analytical data, electronic spectra and magnetic moment results, the structures are suggested as in Fig. 3.

3.3. ESR of copper complexes

The room temperature polycrystalline X-band ESR spectra of [Cu $(H_2L^1)\cdot 4H_2O$], [Cu (H_4L^2) $Cl_2\cdot 6H_2O$], [Cu (H_5L^3) $Cl_2\cdot 3H_2O$] and [Cu $(H_3L^4)\cdot 6H_2O$] complexes gave similar spectral patterns, Fig. 4. All complexes are isotropic in nature with g_s values at 2.14, 2.48, 2.09 and 2.11 and (A) values at 280, 200, 210 and 300, respectively. The spectra show broad signals, which might be due to the polymeric nature of these complexes. These data resulted due to isotropic spectral feature [41,42].

3.4. Thermal analysis

The (DTA) for H_4L^1, H_4L^2, H_5L^3 and H_5L^4 compounds and their complexes are presented in Table 7. The change of entropy, $\Delta S^{\#}$, values for all complexes, are nearly of the same magnitude and lie within the range of (−0.27 to −0.32) kJ K^{-1} $mole^{-1}$. So, the transition states are more ordered, the fraction appeared in the calculated order of the thermal reaction, n, confirmed the reactions proceeded in the complicated mechanisms. The calculated values of the collision parameters, Z, showed a direct relation to E_a [43]. The values of the decomposed substance fraction (α_m), at maximum development of the reaction were calculated. It is nearly with the same magnitude and lies within the range 0.5–0.8. Based on least square calculations, the $\ln \Delta T$ versus $1000/T$ plots for all complexes gave straight lines from which, the activation energies were calculated [44].

DSC is a technique used to study the thermal transitions of a compound, such as glass transitions, crystallization and melting.

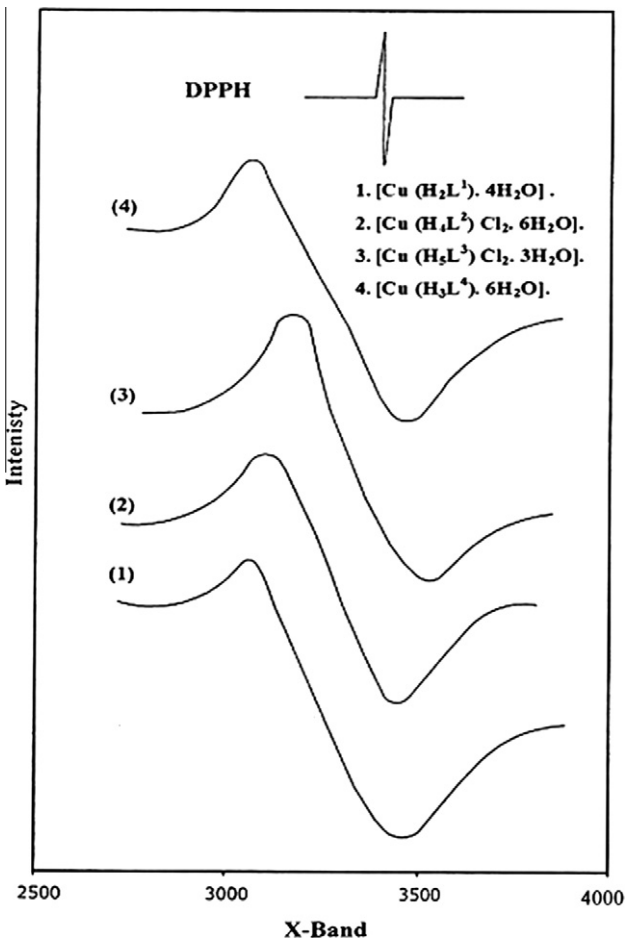

Fig. 4. X-Band ESR spectra of copper complexes.

Table 7
DTA analysis of gallic acid and its azo complexes:

Compound	Type	T_m (K)	ΔE (kJ mol^{-1})	n	α_m	$\Delta S^{\neq}$ (kJ K^{-1} mol^{-1})	$\Delta H^{\neq}$ (kJ mol^{-1})	10^3 (Z s^{-1})
H_4L^1	Endo	397.5	109.1	1.441	0.6	−0.29	−117.2	0.033
	Endo	540.6	439.8	1.206	0.6	−0.29	−156	0.098
	Exo	721.8	50.74	0.501	0.7	−0.31	−225	0.008
Co (H_2L^1)·H_2O	Endo	377.3	55.27	1.491	0.6	−0.3	−113	0.018
	Exo	625	10.3.70	0.864	0.7	−0.3	−189	0.02
	Exo	676.3	225.5	1.029	0.6	−0.3	−201	0.04
	Exo	697	58.92	1.676	0.5	−0.31	−216	0.01
Ni (H_3L^1)$_2$·$4H_2O$	Endo	383.4	37.41	1.385	0.6	−0.3	−116.2	0.012
	Exo	613	101.6	0.616	0.7	−0.3	−185.4	0.02
	Exo	664.1	169.5	2.02	0.5	−0.3	−199	0.031
Cu(H_2L^1)·$4H_2O$	Endo	372.5	18.7	1.627	0.5	−0.31	−115	0.006
	Exo	645.5	193.1	1.61	0.5	−0.3	−192	0.036
H_4L^2	Exo	383	203.9	1.496	0.6	−0.29	−111	0.064
	Exo	833.3	14.37.00	0.492	0.8	−0.32	−270	0.002
	Exo	873	143	2.3	0.5	−0.31	−267	0.02
Co(H_3L^2) (H_4L^2)Cl·$4H_2O$	Exo	373	18.7	1.465	0.6	−0.3	−115	0.006
		658.7	1873	0.957	0.6	−0.31	−209	0.003
Ni (H_3L^2) (H_4L^2) Cl·$4H_2O$	Exo	623.6	459.9	0.658	0.7	−0.29	−181	0.089
	Exo	663	925.3	1.353	0.6	−0.29	−189	0.168
	Exo	723	464.6	1.206	0.6	−0.29	−212	0.077
Cu(H_4L^2)Cl_2·$6H_2O$	Exo	373	20.33	1.543	0.6	−0.31	−115	0.007
	Exo	605	480.9	0.949	0.6	−0.29	−175	0.096
		678	144	0.912	0.6	−0.3	−204	0.026
Ni Cu(H_2L^2)$_2$ (H_4L^2)·$2H_2O$	Exo	373	352.8	1.393	0.6	−0.28	−106	0.114
	Exo	583	82.78	1.373	0.6	−0.3	−177	0.017
	Exo	623	166.1	1.156	0.6	−0.3	−186	0.032
	Exo	663.2	25.73	1.186	0.6	−0.32	−209	0.005
H_5L^3	Exo	373	196	0.55	0.7	−0.29	−108	0.063
	Exo	658.9	4230	1.57	0.5	−0.27	−180	0.771
	Exo	888	1605	1.54	0.6	−0.29	−254	0.217
	Exo	903	24.71	1.69	0.5	−0.32	−290	0.003
Co(H_5L^3) Cl_2·$6H_2O$	Exo	373	95.5	1.94	0.5	−0.29	−110	0.031
	Exo	612.5	179.1	0.85	0.7	−0.3	−182	0.035
Ni (H_5L^3) Cl_2·$6H_2O$	Exo	383	24.4	1.7	0.5	−0.3	117.4	0.008
	Exo	611.4	117.1	0.7	0.7	−0.3	−184.2	0.023
	Exo	693	436.1	1.2	0.6	−0.29	−202.7	0.076
Cu(H_5L^3)Cl_2·$3H_2O$	Exo	546.7	179.1	1.6	0.5	−0.29	−161.8	0.039
H_5L^4	Exo	373	20.5	1.9	0.5	−0.3	−114.7	0.007
	Exo	705	79.2	0.83	0.7	−0.3	−216.4	0.014
	Exo	853.7	383.2	0.86	0.7	−0.29	−253.6	0.054
Co (H_3L^4)·$5H_2O$	Exo	383	39.53	1.608	0.5	−0.3	−116	0.012
	Exo	682.2	68.23	1.182	0.6	−0.31	−210	0.012
Ni (H_3L^4)·$4H_2O$	Exo	652.6	68.2	0.891	0.7	−0.3	−200.3	0.01
Cu (H_3L^4)·$6H_2O$	Exo	555.5	23.86	0.97	0.6	−0.31	−173.8	0.005
	Exo	573	395.5	1.08	0.6	−0.29	166.2	0.083
Cd (H_3L^4)·$2H_2O$	Exo	404.4	30.44	1.163	0.6	−0.31	−124	0.009
	Exo	623	76.28	0.859	0.7	−0.31	−190	0.015
	Exo	738.8	399.9	1.136	0.6	−0.29	−217	0.065

DSC curves are obtained for H_4L^1 and its Ni-complex, Fig. 5, which are done under a flow of N_2 at heating rate 10 °C/min in the temperature range 25–500 °C. It is clear that there are no glass transition temperatures (T_g) for both H_4L^1 and its Ni-complex, where the crystallization temperatures (T_c) for both systems were at 124, 110.7 °C, respectively. The melting temperatures (T_m) are at 449 and 392.6 °C, respectively. The heat capacity can be determined by dividing the heat flow by the heating rate. The variation of C_p versus T can be represented using Debye model as the following relations [45,46]:

$$C_p = \alpha T^3 + \gamma T, \quad \frac{C_P}{T} = \alpha T^2 + \gamma \tag{1}$$

where (a) is the slope of the line and b is the intersection of the line with y-axis (C_p axis), C_p is the specific heat at constant volume, γ is constant equals 10^{-4} cal/g. mole.

According to Debye model [46]:

$$\alpha = \frac{234R}{\theta_D^3}, \quad \theta_D = \sqrt[3]{\frac{234R}{\alpha}}$$

R is the universal gas constant equals 8.3 J/mole/K and θ_D is Debye temperature, which defined as the separate temperature between different temperature. By plotting $\frac{C_p}{T}$ as y-axis and T^2 as x-axis, a straight line is obtained with a slope equals α, also the intersection with y-axis gives the coefficient (γ), Table 8.

3.5. Biological activity study

In this study, four microorganisms representing different microbial categories, Gram-positive (*Staphylococcus aureus*), Gram-negative (*Escherichia coli*, *Pseudomonas aeruginosa)* and one Yeast

Table 8
The slopes and intercept for DSC curves of gallic acid and its Ni-complex.

Compound	$C_p = aT + b$		$\frac{C_p}{T} = \alpha T^2 + \gamma$	
	a	B	γ	A
H_4L^1	0.01	−0.54	−0.225	2×10^{-6}
[Ni (H_3L^1)$_2$·$4H_2O$]	0.03	−8.47	−0.012	2×10^{-7}

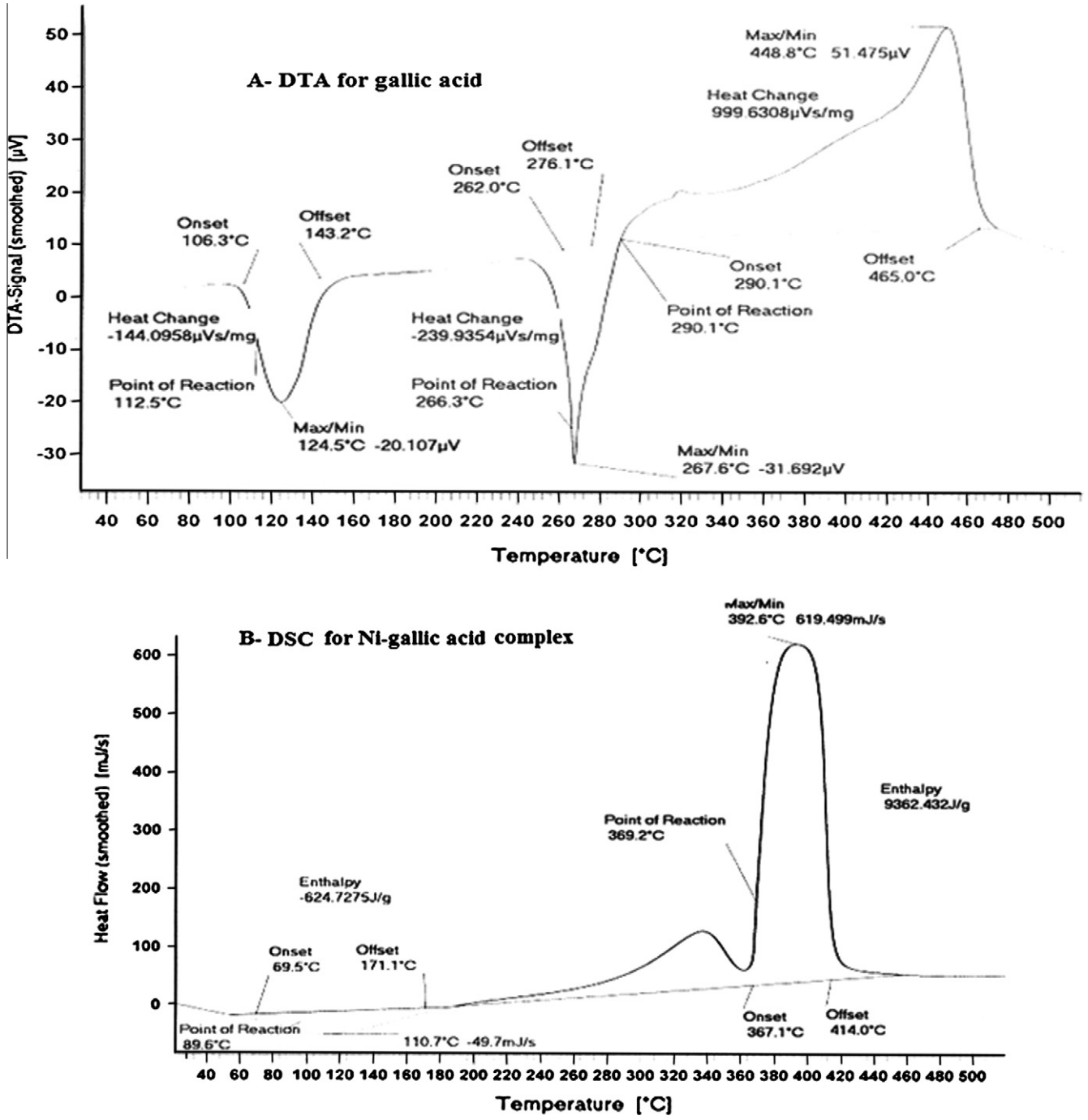

Fig. 5. DTA and DSC curves for gallic acid and its Ni-complex.

Table 9
Biological activities of some selected ligands and their metal complexes.

Compound	G+ bacteria	G− bacteria		Yeast
	Staphylococcus aureus	*Escherichia coli*	*Pseudomonas aeruginosa*	*Candida albicans*
UO_2 (H_2L^1)·2 H_2O	+	+	+	+
H_4L^2	+	–	+	–
Ni $Cu(H_2L^2)_2{\cdot}(H_4L^2){\cdot}2H_2O$	–	–	+	–
H_5L^3	+	–	+	–
$Co(H_5L^3)$ $Cl_2{\cdot}6H_2O$	–	–	+	–
Cu (H_3L^4)·$6H_2O$	–	+	+	–

(*Candida albicans*) were used. The study included six compounds, two legends (H_4L^2 and H_5L^3) and four complexes of different metal ions (Co, Ni Cu mixed metal, Cu and UO_2). The minimum inhibition concentrations (MIC) for the tested compounds were determined

via the double dilution technique [47]. All compounds were dissolved in DMSO. Five concentrations were prepared for each compound (2, 4, 8, 16 and 32 μg/ml). The bacteria were incubated at 37 °C for 24 h in nutrient broth medium, however, the yeast was incubated in malt extract broth for 48 h. MIC was considered at the lowest concentration causing full inhibition of the test organism growth. MIC values for tested compounds for different microorganisms are given in Table 9. The data allow the following observations and conclusions:

(a) *C.* albicans was found to be resistant for all investigated compounds.
(b) It seems that the free legend H_5L^4 is inactive, but its copper complex is of highest activity. So, the copper plays a major role in activity. Compounds with noticeable activity may be considered a start point for development of some new antimicrobial agents.
(c) It is observed that uranyl complex has higher activity [47]. Such increased activity of the metal chelates could be explained on the basis of overtone's concept and chelating theory [47–49]. On chelating, the polarity of the metal ion is reduced to a greater extent due to the overlap of the legend orbital and partial sharing of the positive charge of metal ion with the donor groups. Further, it increases the delocalization of p- and d- electrons over the whole chelate and enhances the lipophilicity of the complex. The increased lipophilicity enhances the penetration of the complexes into lipid membranes and blocking of metal binding sites on the enzymes of the microorganism.

4. Conclusion

Gallic acid and its azo derivatives were of distinctive behavior. This is because the variety of the geometry of their formed complexes. This was reflected in various studies, such as thermal analysis and biological activity. Due to the lack of publishing about these complexes, we recommend to do intensive studies of the current work subject to explore all the characteristics of such complexes and the possibility of applied use.

References

[1] D. Rajalakshmi, S. Narasimban, D.L. Madhavi, S.S. Deshpande, D.K. Salunkhe, Food Antioxidants: Sources and Methods of Evaluation, Food Antioxidants, Marcel Dekker, New York, 1996. pp. 65–157.
[2] M.A. Bianco, H. Savolainen, J. Sci. Total. Environ. 203 (1997) 79–82.
[3] J.M. Gil, M.C.R. Snchez, F.J.M. Gil, M.J. Yacamn, J. Chem. Educ. 83 (2006) 1476–1478.
[4] G.M. Elvira, S. Chandra, R. M.M. Vinicio, W. Wenyi, Food Chem. Toxicol. 44 (2006) 191–1203.
[5] H.C. Lan, L.Y. Charn, Y.G. Chin, C.H. Yin, Food Chem. 103 (2007) 528–535.
[6] J. Kinjo, T. Nagao, T. Tanaka, G. Nonaka, M. Okawa, T. Nohara, H. Okabe, J. Biol. Pharm. Bull. 25 (2002) 1238–1240.
[7] K. Jittawan, Food Chem. 110 (2008) 881–890.
[8] R.F. Hurrell, M. Reddy, J. Nutr. 81 (1999) 289–295.
[9] J.D. Cook, M.B. Reddy, R.F. Hurrell Am, J. Clin. Nutr. 61 (1995) 800–804.
[10] N. Okabe, H. Kyoyama, M. Suzuki, J. Acta Cryst. Sect. E57 (2001) o764–o766.
[11] N. Fatima, Z.T. Maqsood, S.A. Kazmi, J. Chem. Soc. Pac. 24 (2002) 49–56; 20 (1998) 295–298.
[12] A.S. Li, B. Bandy, S.S. Tsang, A.J. Davison, J. Free Rad. Res. 33 (2000) 551–566.
[13] R.B. Sorkaz, I. Mazol, J. Biosci. 49 (2000) 881–894.
[14] M.D. Agarwal, C.S. Bhandari, M.K. Dixit, N.C. Sogani, J. Inst. Chem. 49 (1977) 124–126.
[15] M.S. Masoud, A.F. El-Husseiny, M.M. Abd El-Ghany, H.H. Hammud Bull, Fac. Sci. Alex. Univ. 44 (2006) 41–54.
[16] E. Kissinger, Anal. Chem. 29 (1957) 1702–1706.
[17] M.S. Masoud, T.S. Kasem, M.A. Shaker, A.E. Ali, J. Therm. Anal. Calorimetr. 84 (2006) 549–555.
[18] M.S. Masoud, S.A. Abou El-Enein, H.A. Motoweh, A.E. Ali, J. Therm. Anal. Calorimetr. 75 (2004) 51–61.
[19] M.L. Dhar, O. Singh, J. Therm. Anal. 37 (1991) 259–266.
[20] E. Koch, Thermochim. Acta 94 (1985) 43–46.
[21] A.J. Ivana, V.S. Zoran, S.D. Enis, M.N. Jovan, J. Nano Scale Res. Lett. 5 (2010) 81–88.
[22] A. Kula, J. Therm. Anal. Calorimetr. 75 (2004) 79–86.
[23] M.S. Masoud, E.A. Khalil, A.M. Hindawy, A.M. Ramadan, Can. J. Anal. Sci. Spectrosc. 50 (2005) 175–188.
[24] A.T.T. Hsieh, R.M. Sheahan, B.O. West, Aust. J. Chem. 28 (1975) 885–891.
[25] S.P.M. Glynn, J.K. Swith, J. Mol. Spectra 6 (1961) 164–172.
[26] L.H. Jones, Spectrochim. Acta 15A (1959) 409–411.
[27] M.B.H. Howlader, M.S. Islam, M.R. Karim, Indian J. Chem. 39A (2000) 407–409.
[28] A. Sreekanth, M. Joseph, H.K. Fun, M.R.P. Kurup, Polyhedron 25 (2006) 1408–1411.
[29] M.S. Masoud, E.A. Khalil, A.M. Ramadan, Y.M. Gohar, A. Sweyllam, Spectrochim. Acta 67A (2007) 669–677.
[30] M.S. Masoud, H.A. Motaweh, A.E. Ali, Indian J. Chem. 40A (2001) 733–737.
[31] P.G. Prakash, J.L. Rao, J. Mater. Sci. 39 (2004) 193–200.
[32] U. El- Ayaan, M.M. Youssef, S. Al-Shihry, J. Mol. Struct. 936 (2009) 213–219.
[33] F. Billes, I.M. Ziegler, P. Bombicz, J. Vib. Spectrosc. 43 (2007) 193–202.
[34] I.M. Ziegler, F. Billes, J. Mol. Struct. 618 (2002) 259–265.
[35] D. Slawins Ka, K. Polewski, P. Role Wski, J. Slawin Ski, J. Int. Agrophys. 21 (2007) 199–208.
[36] M.S.E. Ali, E.M. Fawzy, Spectrochim Acta. 60A (2004) 2807–2817.
[37] M.S. Masoud, A.E. Ali, R.H. Mohamed, A.A. Mostafa, Spectrochim. Acta 62A (2005) 114–2119.
[38] M.M. Aly, N.I. Al-Shatti, Trans. Met. Chem 23 (1998) 361–369.
[39] H.A. Dessouki, H.M. Killa, A. Zaghloul, Spectrochim. Acta 42A (1986) 631–635.
[40] M.S. Masoud, G.B. Mohamed, Y.H. Abdul Razek, A.E. Ali, F.N. Khiry, Spectrochim. Lett. 35 (2002) 377–413.
[41] M.S. Masoud, G.B. Mohamed, Y.H. Abdul-Razek, A.E. Ali, F.N. Khairy, J. Kor. Chem. Soc. 46 (2002) 99–116.
[42] M.S. Masoud, Chemistry 40 (2010) 1–4.
[43] M.S. Masoud, A.A. Soayed, A.E. Ali, Spectrochim. Acta 60A (2004) 1907–1915.
[44] R. Iordanova, E. Lefterova, I. Uzunov, Y. Dimitriev, D. Klissurski, J. Therm. Anal. Calorimetr. 70 (2002) 393–404.
[45] M.S. Celej, S.A. Dassie, M. Gonzalez, M.L. Bianconi, G.D. Fidelio, J. Anal. Biochem. 350 (2006) 277–284.
[46] H. Mcphillips, D.Q. Craig, P.G. Royall, V.L. Hille, Int. J. Pharm. 180 (1999) 83–90.
[47] B.G.S. Bodeis, R.D. Walker, D.G. White, S. Zhao, P.F. Mcdermott, J. Meng, J. Antimicrob. Chemother. 50 (2002) 487–494.
[48] E. Canpolat, M. Kaya, S. Gur, Tur. J. Chem. 28 (2004) 235–242.
[49] B.G. Tweedy, Phytopathology 55 (1964) 910–914.